Research on Chemical Intermediates (2021) 47:743–757
https://doi.org/10.1007/s11164-020-04296-4

Methane conversion to higher value-added product and energy co-generation using anodes OF PdCu/C in a solid electrolyte reactor: alkaline fuel cell type monitored by differential mass spectroscopy

C. M. Godoi[1] · M. C. L. Santos[1] · A. J. Silva[1] · T. L. Tagomori[1,2] · A. S. Ramos[1] · R. F. B. de Souza[1] · A. Oliveira Neto[1]

Received: 12 August 2020 / Accepted: 8 October 2020 / Published online: 27 October 2020

Abstract

Pd_xCu_y/C catalysts combinations were employed to CH_4 partial oxidation in mild condition using a solid electrolyte reactor—alkaline fuel cell type. The differential mass spectroscopy on line method was used to monitor the oxidation products obtained as methanol, dimethyl ether, methyl formate and potassium formate. It was observed that as the electrical potential of the reactor increases, the generation of products decreases. The best results for conversion of methane into methanol and energy co-generation was obtained from $Pd_{90}Cu_{10}/C$ and $Pd_{50}Cu_{50}/C$ due to better H_2O activation effects and adsorption site for CH_4 oxidation.

Keywords Solid electrolyte reactor · Methane into products · PdCu/C · Methane partial oxidation

Introduction

Methane is the major component of natural gas, and the second most abundant greenhouse gas after CO_2, but is the most potent in trapping heat having a detrimental impact on the atmosphere. To mitigate the greenhouse effects of this gas, which is gaining importance as a source of primary energy, research groups are looking for

✉ A. Oliveira Neto
aolivei@ipen.br

R. F. B. de Souza
aolivei@ipen.br

[1] Instituto de Pesquisas Energéticas E Nucleares, IPEN/CNEN-SP, Av. Prof. Lineu Prestes, 2242 Cidade Universitária, São Paulo, SP CEP 05508-000, Brazil

[2] Faculdades Oswaldo Cruz, R. Brg. Galvão, 540 - Metrô Marechal Deodoro, São Paulo, SP 01151-000, Brazil

ways to convert CH_4 into higher value-added products and that they are not directly dispersed in the atmosphere [1–3].

There are different strategies to carry out this conversion, among them are the thermal reform [4], the photocatalytic conversion [5] and electrochemical routes [6, 7]; these routes usually need an energy injection in the system to occur. Therefore, strategies that promote the conversion of methane into higher value-added products with co-generation of energy become an advance [2, 8].

However, although the methane reactions have high activation energy and have low efficiency [9, 10], the key to generating higher value-added products is partial oxidation of methane. These reactions lead to formation of methyl radicals by water activation, in mild conditions, to generating HO· species [11–15]. These radicals activate the methane C–H bond scission, leading to the formation of reactive methyl radical and hydrogen, which in turn, reacts with water molecules to produce other products such as methanol.

Among the different electrochemical routes, it is possible to couple oxidation and reduction reactions in different compartments of a reactor, generating a potential difference and, therefore, the possibility of chemical and energy co-generation. In this sense, the application of low-temperature fuel cells for partial oxidation of methane at mild conditions has been studied [2, 16, 17], and the most usual products in these works are the methanol and formate species [17]. Recently, many experimental studies on the anion exchange membrane (AEM) fuel cell have been carried out to investigate the operating behavior with various cell designs and different operational conditions for co-generation of electricity and valuable chemicals [2, 18].

The study by Santos [2] indicated that Pd is a promising metal for partial oxidation of methane under mild conditions in a solid electrolyte reactor—alkaline fuel cell type (SER-AFC), and, when combined with Cu as a second metal for electronic exchange state surface, it is possible that catalyst poisoning will decrease and catalyst activity and lifetime will increase [19]. Copper has been shown to be active for the partial oxidation of methane to methanol; this metal is very active for water dissociation in 450–500 K [20], due to the formation of oxygen vacancy in copper oxides that can activate water oxygen and C-H methane bond [21–23].

Therefore, the addition of copper to palladium can be a promising proposal once it is known that this metal and its oxidation states can easily vary between Cu^0, Cu^+ and Cu^{2+} and improve the activity and electrocatalytic stability and facilitate oxidative desorption for product generation [24–26]. In this context, the aims of this work were to determine which proportions of Cu combined with Pd catalyst would increase the water activation, improving the methane oxidation rate in alkaline media, in order to increase the methanol generation, as well as to verify if the increase in the oxidation rate would lead to greater power in the fuel cell.

Experimental

Binary Pd_xCu_y catalytic systems and their different atomic compositions were prepared by sodium borohydride ($NaBH_4$—Aldrich) reduction method using as metal sources, palladium ($Pd(NO_3)_2{\cdot}2H_2O$—Aldrich) and copper ($CuCl_2{\cdot}2H_2O$—Aldrich)

with 20 wt% of metal loading and using Vulcan Carbon (XC72) as support. The metal mixture was dissolved in water/2-propanol 50/50 (*v/v*). The excess sodium borohydride solution with 10 mL 0.01 mol L^{-1} of KOH was added to the metal mixture. The catalysts were washed with water with vacuum filtered and dried at 70 °C for 2 h.

The micrographs from transmission electron microscopy (TEM) were obtained using a JEOL JEM-2100 electron microscope, operated at 200 kV. One hundred fifty nanoparticles of each catalyst were averaged digitally for histogram construction. The X-ray diffraction (XRD) was obtained using a diffractometer model Miniflex II, with Cu kα radiation source of 0.15406 Å, set at 2θ range 20°–90º, with 2 min^{-1} scan speed.

Cyclic voltammetry (CV) and rotating ring disk electrode (RRDE) to electrochemical measurements were performed using a three-electrode cell in an Ametek Parstat 3000A-DX bipotentiostat/galvanostat and an RRDE (Pine Instruments) composed of a gold ring (area = 0.19 cm^2) and a glassy carbon disk (area = 0.25 cm^2) with collection factor of 0.38. The electrochemical experiments were performed in nitrogen-purged environment; Ag/AgCl electrode (3 mol L^{-1} KCl) was used as a reference electrode, and a platinum plate (area = 2 cm^2) was used as a counter electrode in a static state. On the surface of the working electrodes, 15 µL aliquots of each sample previously prepared with a paint composed of a mixture of 8 mg of catalyst + 750 µL of H_2O, 250 µL of isopropyl alcohol and 15 µL of 5% Nafion D-520 were added. All experiments with different catalysts were performed in 1 mol L^{-1} KOH medium. The curves of rotation ring disk were obtained at different speeds ranging from 100, 400, 600, 900, 1600 and 2500 rpm.

The polarization curves of SER-AFC were obtained using a cell with Electro-Chem unit-type serpentine distribution as reactor supplied by CH_4 (flow rate of 50 mL min^{-1}) and 1.0 mol L^{-1} KOH (1 mL min^{-1}) at room temperature at the anode and O_2 with flow of 400 mL min^{-1} and humidifier bottle at controlled temperature 80 °C at the cathode. The membrane electrode assembly (MEA) was constituted by *Nafion*® 117 membrane that was maintained in alkaline medium (KOH 6 M) per 24 h after the cell test; cathode was formed by Pt/C BASF catalyst (20% by weight) with 1 mg cm^{-2} and catalysts with different PdCu ratios (20 wt%) as anode.

The reactional products resultants from anodic effluent output from the SER-AFC were analyzed by online differential mass spectrometry (DMS), a quadrupole mass spectrometer, 100 DA QMS 200 M1, Prisma, Pfeiffer® equipped with continuous dynode secondary electron multiplier/Faraday cup detector with sensitivity of 200 A $mbar^{-1}$ and two differentials pumped chambers: a primary vacuum chamber was pumped with a rotary vane pump (DUO 5, Pfeiffer) and the secondary chamber was pumped turbomolecular pump backed by a dry diaphragm pump (hi-cube 80, Pfeiffer®). An interface was adapted on top of the primary vacuum chamber separated by a PTFE membrane (pore size 200 nm Whatman®) in continuous flow, and anodic reaction products were collected by 300 s increments of 100 mV monitoring by multiple ion detection (MID). The ionic current results were expressed as chemical fragments (*m/z*) as a potential function.

The products were collected from AEMFC effluent by 300 s increments of 100 mV and analyzed by ATR-FTIR performed on an ATR accessory (MIRacle

with a ZnSe Crystal Plate Pike®) installed on a Nicolet® 6700 FT-IR spectrometer equipped with a cooled MCT detector with N_2 liquid. The quantification of methanol was developed by Boyaci's method with Raman spectroscopy [2, 27], using Horiba Scientific MacroRam Raman spectroscopy equipment. The calibration curve was constructed from standard methanol solutions 1 mol L^{-1} (HPLC degree) followed by eight successive dilutions. The wavelength was set at 785 nm. The results were expressed as mol L^{-1} h^{-1}.

Results and discussion

Figure 1 shows the X-ray diffractograms of the Pd_xCu_y/C electrocatalysts and different proportions. For all materials, it is possible to observe the presence of the plane (002) at approximately $2\theta = 25°$, associated with the hexagonal structure of the carbon support (JCPDS # 50–926). For Pd structure, it is possible to identify peaks at $2\theta \approx 40°$, 46°, 67°, 82° and 86° associated with the crystalline planes (111), (200), (220), (311) e (222), respectively, indicating these catalysts have prevailed face-centered cubic (FCC) structure according to (JCPDS # 89-4897).

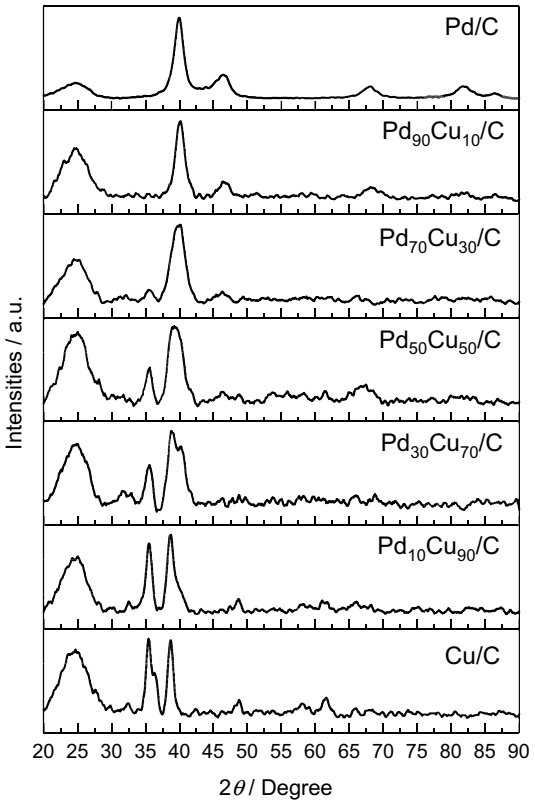

Fig. 1 X-ray diffraction pattern of Pd/C and PdCu/C electrocatalysts in different atomic compositions

For materials with copper amounts above 30%, there is an enlargement and subsequent separation in 2 peaks (for Cu > 70%) at a band closure to $2\theta \approx 40°$; relative to the plane (111) of the Pd, this second peak is relative to the face (200) of the Cu_2O phase (JCPDS # 05-0667). This phase also presents itself in the peaks in $2\theta \approx 36°$ (111) and 62° (220). The peak that shows the presence of CuO related to the plane (111) is close to $2\theta \approx 35°$. XRD patterns for the sample values are in accordance with JCPDS # 05-0667 and JCPDS # 45-0937, so there is a probability of arguing the existence of mixed CuO and Cu_2O on the sample surface [28]. It should be noted that in the samples with a higher concentration of copper the formation of oxides is more apparent due to the high affinity with nanometric copper by oxygen [29].

In micrographs obtained by TEM illustrated in Fig. 2, the Pd_xCu_y/C electrocatalysts and their different prepared proportions present good dispersion with some regions of agglomerations on the carbon support, characteristics inherent to the reduction method via sodium borohydride. The distribution histogram fit presents average sizes of the nanoparticles about the range of 6.1 nm, 9.2 nm, 7.2 nm, 7.0 nm and 8.0 nm for Pd/C, $Pd_{90}Cu_{10}/C$, $Pd_{70}Cu_{30}/C$, $Pd_{50}Cu_{50}/C$ and $Pd_{30}Cu_{70}/C$, respectively. These values are close to the values obtained by other studies as reported in the literature [2, 24, 30] and promising for electrocatalysis. For the $Pd_{10}Cu_{90}/C$ and Cu/C systems, it was not possible to explain the nanoparticle count size, since the micrograph shows regions with high agglomeration that may be associated with Cu_2O [31]. The high concentration of copper seems to have an influence on the dispersion of bimetallic electrocatalysts, causing aggregation with a heterogeneous structure named displacement densities [32].

In the cyclic voltammetry (Fig. 3), it is possible to observe the hydrogen adsorption/desorption region on Pd (−0.85 V to −0.6 V) losing its definition with the increase in copper incorporated in the Pd. For compositions with copper amounts above 50%, it is practically no longer possible to observe the characteristic profile of Pd. In $Pd_{50}Cu_{50}/C$ is observed a peak at ≈ −0.19 V corresponding to pair $Cu_2O/Cu(OH)_2$ [33, 34]; The Cu/C electrocatalyst showed a peak in −0.6V, which could be associated to Cu oxides spicies, however this peak is shifted to lower potentials in comparison with $Pd_{30}Cu_{70}/C$ and $Pd_{10}Cu_{90}/C$; for these four materials, it is also possible to observe a peak close to −0.45 V corresponding to the pair Cu/Cu_2O [33].

For the partial oxidation of methane, the literature indicates that the presence of the OH radical is important [12, 15]; electrochemical experiment is able detect this radical by the existence of H_2O_2 in solution [35] (Eq. 1); thus, rotation ring disk measurements were performed to observe the generation and detection process of H_2O_2 during the electrode redox process in function of potential, as reported by Garcia et al. [36]. In Fig. 4 was presented the ring-disk curves at 1600 rpm. The $Pd_{50}Cu_{50}/C$ catalysts presented the most promise to HO· production, and Pd/C presents the lower current for H_2O_2 generation.

$$\cdot OH + \cdot OH \rightarrow H_2O_2 \text{ or } HO_2^{-1} \quad \text{in alkaline medium} \tag{1}$$

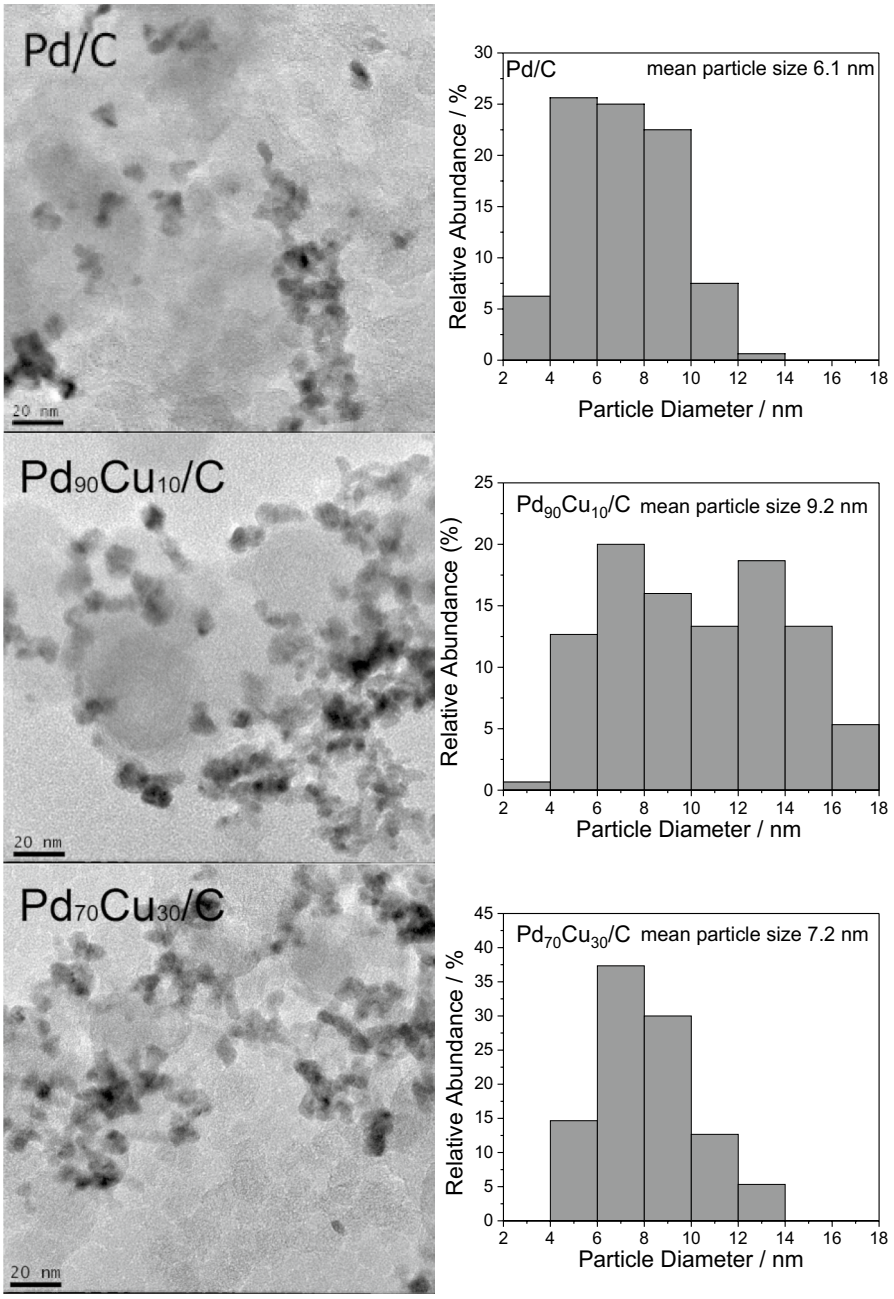

Fig. 2 TEM micrographs obtained from Pd_xCu_y/C electrocatalysts in different compositions supported on carbon

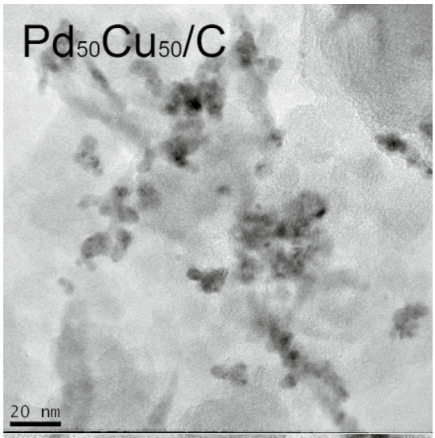

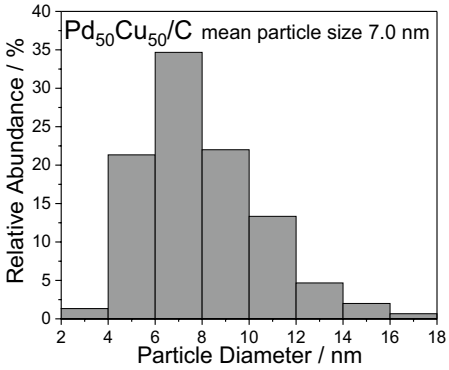

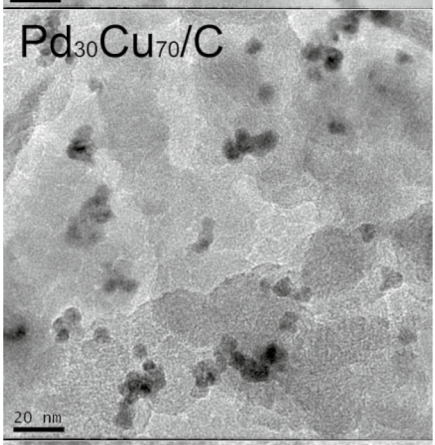

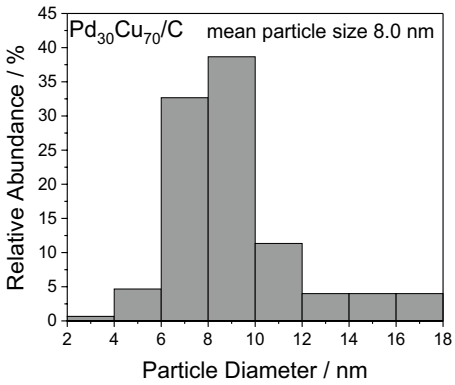

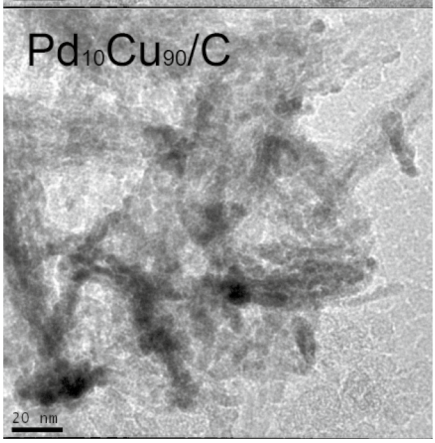

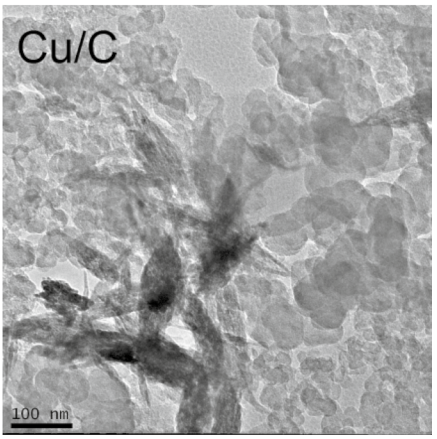

Fig. 2 (continued)

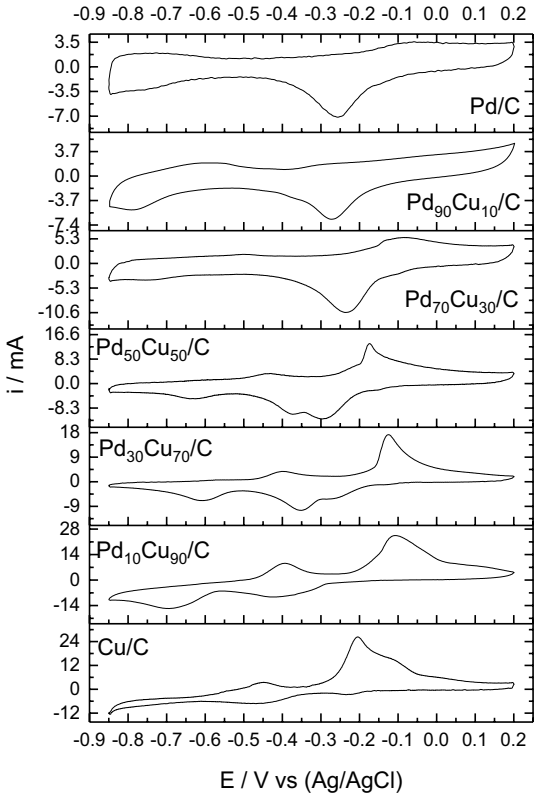

Fig. 3 Cyclic voltammetry curves of the PdCu electrodes in different proportions (scan rate $v = 10$ mV s^{-1}) in 1 mol L^{-1} KOH

However, only the ring-disk curves are no determinant for H_2O_2 when compared different materials, due charge transfer resistance. Due to this, the selectivity for the formation of peroxide (% H_2O_2) can be calculated by Eq. (2) [37]:

$$H_2O_2\% = \frac{200I_r/N}{I_d + I_r/N} \tag{2}$$

where I_d is the disk current, I_r is the ring current, and N is the RRDE collection efficiency (0.38%). The results (Fig. 5) showed that where the H_2O_2% lines in each potential range from −0.8 to −0.2 V, the average H_2O_2 production varies by ~ 12 %, ~ 8%, ~ 4.7%, ~ 4.2%, ~ 4%, ~ 3%, and ~ 1.7% for $Pd_{50}Cu_{50}$/C, Cu/C, $Pd_{90}Cu_{10}$/C $Pd_{30}Cu_{70}$/C Pd/C, $Pd_{70}Cu_{30}$/C, and $Pd_{10}Cu_{90}$/C, respectively.

The electrochemical curves obtained from SER-AFC represent the methane oxidation in anodic chamber feed by a mixture of methane (room temperature) and an aqueous solution of KOH 1 mol L^{-1} catalyzed by different proportions of Pd and Cu supported on carbon. In Fig. 6 it is possible to observe that the higher current is measured for $Pd_{50}Cu_{50}$/C and Cu/C, the same materials that showed the highest selectivity for generation of hydrogen peroxide. The value of our OCV

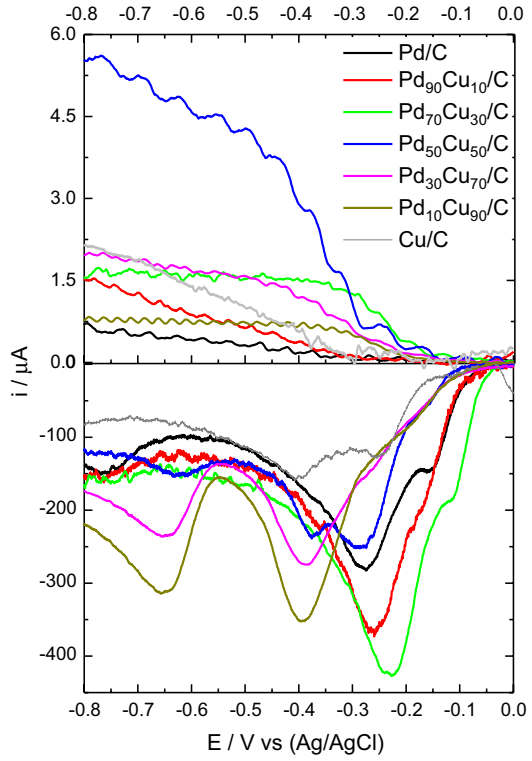

Fig. 4 RRDE voltammograms at 1600 r.p.m. in O_2-unsaturated electrolyte with the disk current, ring current and current corresponding to hydrogen peroxide obtained from the ring current

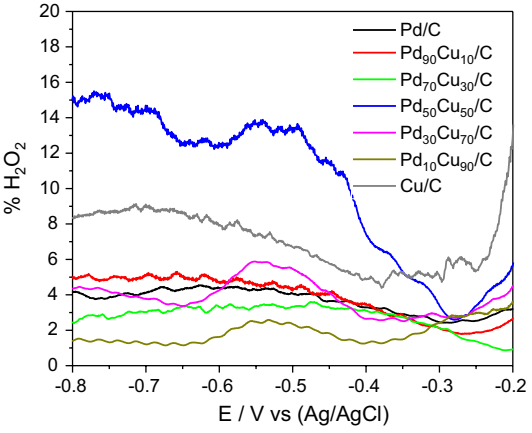

Fig. 5 H_2O_2% selectivity as a function of the applied potential (E)

is comparable to the one reported in the literature for methane oxidation at low-temperature fuel cells (about 0.3–0.4 V) [2, 16, 38–40].

Figure 7 shows current ionic (I_i) of effluent of the reactor SER-AFC measured by DMS for identification of products from partial methane oxidation. The I_i to $m/z = 32$, attributed to methanol, showed a signal increase of OCV to 0 V to

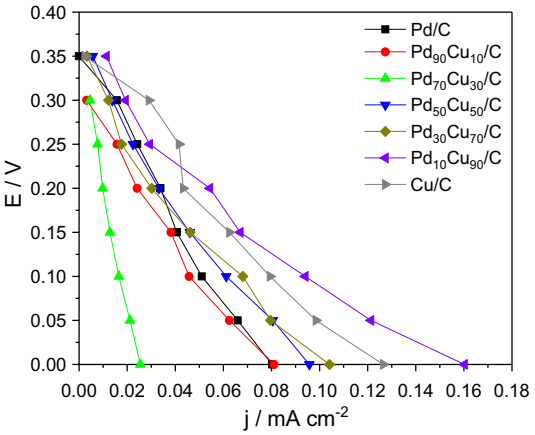

Fig. 6 Polarization curves of a 5 cm^2 SEMR-AFC at room temperature using PdCu/C catalysts anode (5 mg cm^{-2} catalyst loading) and Pt/C Basf for the cathode in all experiments (1 mg Pt cm^{-2} catalyst loading with 20 wt% Pt loading on carbon), Nafion 117 membrane KOH treated; KOH 1.0 mol L^{-1} + CH_4 50 mL min^{-1} and O_2 flux of 200 mL min^{-1}

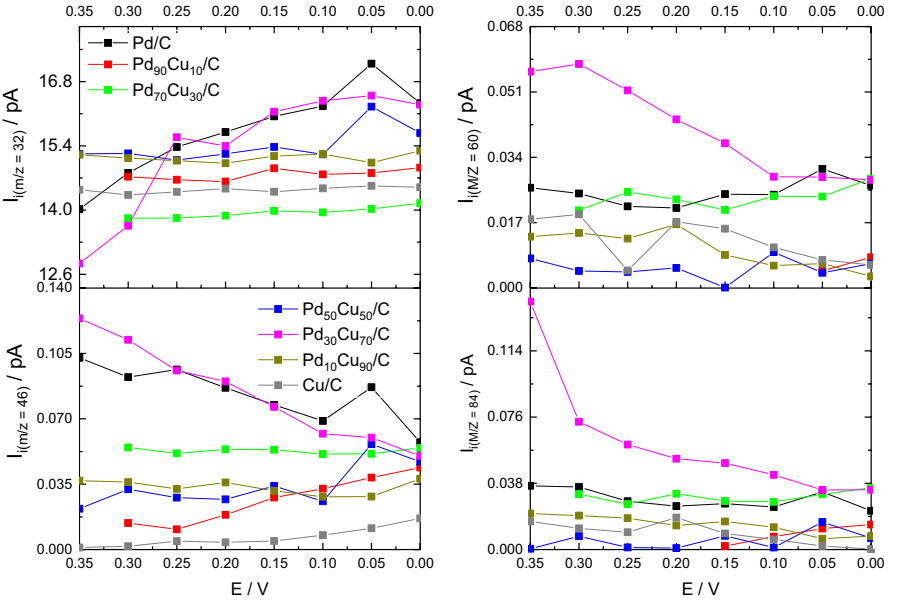

Fig. 7 DMS represented as ion current (I_i) of chemical species obtained by the partial oxidation of methane for all Pd_xCu_y catalysts obtained in different potentials (0.35 to 0.0 V)

materials Pd/C, $Pd_{50}Cu_{50}$/C and $Pd_{30}Cu_{70}$/C; besides, the same material shows a declining trend between 0.05 and 0 V, which may be an indication of the oxidation of alcohol to another product. For $m/z = 46$ that can be attributed for ethanol and/or dimethyl-ether; for this signal, four different behaviors are observed: (1) signal increasing with decreasing potential observed in Cu/C, $Pd_{90}Cu_{10}$/C and $Pd_{50}Cu_{50}$/C; (2) signal exists almost without variation from 0.3 to 0.1 V, and at 0.05 to 0 the signal increases significantly, observed for $Pd_{50}Cu_{50}$/C; (3) for

$Pd_{70}Cu_{30}$/C and $Pd_{10}Cu_{90}$/C materials, the signal do not show significant variation with the potential variation; and (4) the decrease along with the potential, as observed for Pd/C and $Pd_{30}Cu_{70}$/C.

The signal with $m/z = 60$ is attributed to methyl formate; this signal increases with the decrease in the potential for the materials most enriched with Pd (Pd/C, $Pd_{90}Cu_{10}$/C and $Pd_{70}Cu_{30}$/C); for $Pd_{50}Cu_{50}$/C, the signal does not undergo significant changes throughout the range of potentials, while for Cu-enriched materials, this signal decreases with potential. For potassium formate ($m/z = 84$), that decreases from the OCV to 0 V, except for Pd/C, $Pd_{90}Cu_{10}$/C, $Pd_{70}Cu_{30}$/C and $Pd_{50}Cu_{50}$/C that increases indicating that the materials with high concentration of adsorption sites and some points near these sites can produce more oxidized molecules with current increment.

The DMS shows the profile of the species due to the partial oxidation of methane; however, in many cases, the I_i can be associated with more than one chemical species. Therefore, SER-AFC effluent samples were also analyzed by infrared spectroscopy (Fig. 8); it is possible to observe characteristic bands of each chemical species as a function of potential. It was noted that with decreasing potential, the centralized band by ~ 1302 cm^{-1} increases, corresponding to the deformation of methane [2, 8]. This behavior can be explained by the solubility of methane in aqueous KOH solution, provided by the increase in small organic molecules formed from the partial oxidation of the hydrocarbon [2].

Methanol production is evidenced by bands of 1033, 1077 and 1082 cm^{-1} [2, 8] analyzing the FTIR spectra. These signals appear for all materials in all potentials and follow the behavior observed for $m/z = 32$ (Fig. 7), except for the 1030 cm^{-1} band that appears larger for the $Pd_{70}Cu_{30}$/C, $Pd_{50}Cu_{50}$/C, $Pd_{30}Cu_{70}$/C and Cu/C where there is another band centered on 1017 cm^{-1} convoluted. In DMS experiments was observed the I_i for $m/z = 46$ attributed to ethanol and/or dimethyl ether; however, in the FTIR spectra, ethanol fingerprint bands were not observed but the band at 1232 cm^{-1} was observed corresponding to CH_3 rock [41] of the dimethyl ether. This band appears in all spectra in all potentials, especially on Pd/C and $Pd_{30}Cu_{70}$/C, which presents a strongly decreasing profile along with the potential, as observed for the I_i of $m/z = 46$. The band centered at ~ 1344 cm^{-1} correspond to the ν (COO) of the formate in the solution [42–44] is detected for all materials containing Pd; nevertheless in $Pd_{70}Cu_{30}$/C catalyst, this band increases with decreasing potential as observed in DMS measurements, probably due to the oxidation reaction of methanol. The carbonate bands (~ 1382 cm^{-1}) are observed only for $Pd_{50}Cu_{50}$/C and Cu/C, indicating total oxidation of methane. This behavior is associated with decreasing of methanol production observed by DMS, which may be an explanation for the higher current obtained in the polarization curves.

The rate reaction (r) of methanol produced in the SER-FC can be quantified by the Boyaci's method [36]. Figure 9 shows the amount of methanol concentration as a function of potential. The sample was collected using an analytical curve built in the concentration range of 0.005–1.000 mol L^{-1} of methanol, at the obtained intensity = 4.249 + 4.037 [CH_3OH] with a correlation coefficient of 0.962. The rate reaction (r) is calculated by Eq. (3)

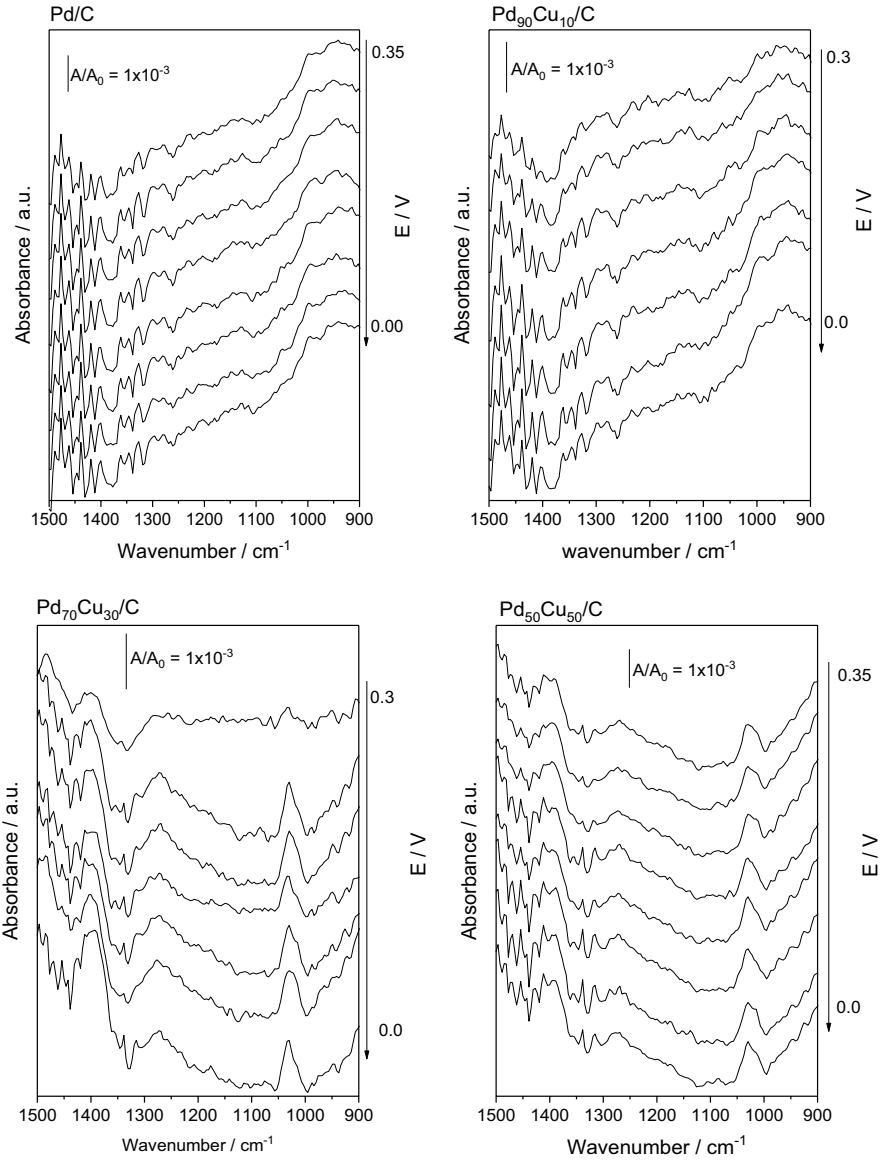

Fig. 8 FTIR spectra in situ collected at different potentials in KOH 1.0 mol L^{-1} with methane flow adjusted to 100 mL min^{-1} for all catalysts

$$r = \frac{\text{Methanol}_{\text{amount}}}{\text{Volume} \times \text{Time}} \tag{3}$$

The results of (r) for Pd/C are in congruence with patterns observed in DMS measures. The addition of Cu in the proportion raises the rate reaction for methanol production, mainly for $Pd_{50}Cu_{50}$/C and $Pd_{90}Cu_{10}$/C materials, which are among the

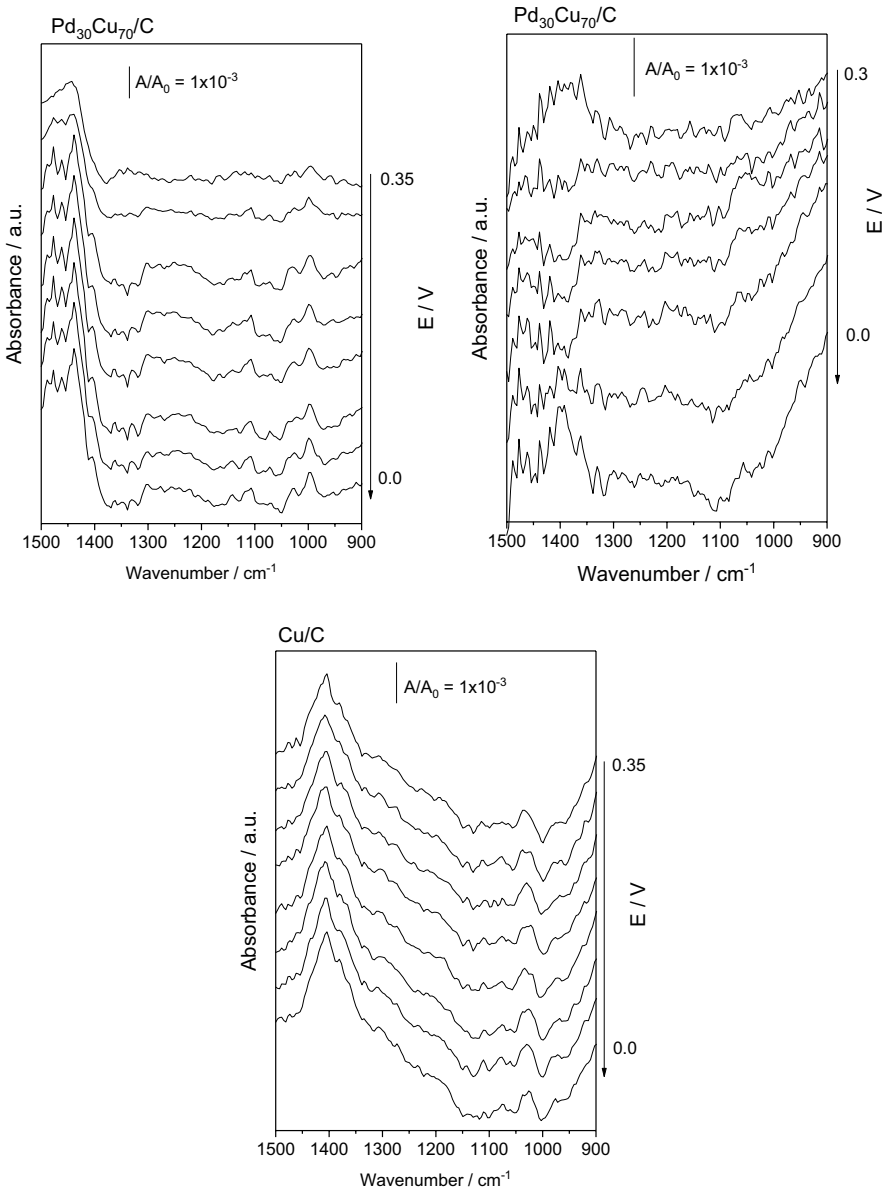

Fig. 8 (continued)

most selective materials for the generation of peroxide, as discussed in Fig. 5 and reported by Garcia and co-workers [36]. Cu/C showed very low methanol production, indicating the adsorption site lack to water activating. Another important point is that the phase difference of copper-containing catalysts shows not only one optimal point for partial methane oxidation but two, one in $Pd_{90}Cu_{10}$/C which is probably due to the amount of adsorption sites on the Pd and the water content, and a

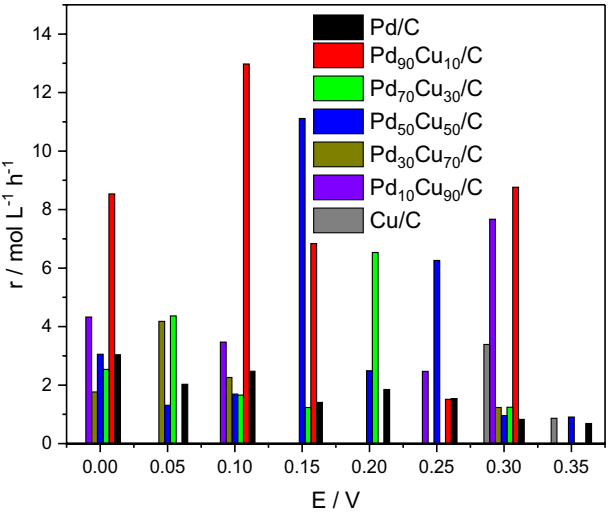

Fig. 9 Rate reaction of all Pd_xCu_y/C catalysts to methanol generation

second in $Pd_{50}Cu_{50}/C$ where, although the Pd sites are in smaller numbers, we have the CuO and Cu_2O phases operating complementarily in the water activation.

Conclusion

The use of SER-AFC for conversion of CH_4 to organic added-value products with energy co-generation is promising. Characterization techniques such as XRD and TEM indicated oscillation in the electrocatalytic structure associated with the formation of copper oxides such as CuO and Cu_2O also confirmed in the anodic scan presented by CV. The catalyst most active for energy generation presents signals of conversion total of CH_4 too, and, for the conversion of hydrocarbon to alcohol, water activation (CuO and PdO) is required and also adsorption sites as Pd. In both cases, the materials with grater water activation are important; in this study, these materials were $Pd_{90}Cu_{10}$, $Pd_{50}Cu_{50}/C$ and Cu/C. Besides methanol, dimethyl-ether and methyl formate were also detected, important solvents for industry, that can have their synthesis favored both with the variation of the amount of Cu in the catalyst and in the potential of the operation of the SER-AFC.

Acknowledgements We are grateful to CAPES, CNPq 300816/2016-2), FAPESP (2014/09087-4, 2014/50279-4 and 2017/11937-4) and CINE-SHELL (ANP)/FAPESP Grants 2017/11937-4 for financial supports.

References

1. M. Subrahmanyam, S. Kaneco, N. Alonso-Vante, Appl. Catal. B **23**, 169 (1999)

2. M.C.L. Santos, L.C. Nunes, L.M.G. Silva, A.S. Ramos, F.C. Fonseca, R.F.B. de Souza, A.O. Neto, ChemistrySelect **4**, 11430 (2019)
3. J. Jang, K. Shen, C.G. Morales-Guio, Joule **3**, 2589 (2019)
4. V.L. Sushkevich, J.A. van Bokhoven, Catal. Sci. Technol. **10**, 382 (2020)
5. J. Yang, J. Hao, J. Wei, J. Dai, Y. Li, Fuel **266**, 117104 (2020)
6. A. Tomita, J. Nakajima, T. Hibino, Angew. Chem. Int. Ed. **47**, 1462 (2008)
7. R.S. Rocha, L.M. Camargo, M.R.V. Lanza, R. Bertazzoli, Electrocatalysis **1**, 224 (2010)
8. J. Nandenha, R.M. Piasentin, L.M.G. Silva, E.H. Fontes, A.O. Neto, R.F.B. de Souza, Ionics **25**, 5077 (2019)
9. Y. Gambo, A.A. Jalil, S. Triwahyono, A.A. Abdulrasheed, J. Ind. Eng. Chem. **59**, 218 (2018)
10. S. Lim, J.-W. Choi, D.J. Suh, K.H. Song, H.C. Ham, J.-M. Ha, J. Catal. **375**, 478 (2019)
11. O.B. Ayodele, Energy Convers. Manag. **126**, 537 (2016)
12. L. Arnarson, P.S. Schmidt, M. Pandey, A. Bagger, K.S. Thygesen, I.E.L. Stephens, J. Rossmeisl, Phys. Chem. Chem. Phys. **20**, 11152 (2018)
13. A. Hameed, I.M.I. Ismail, M. Aslam, M.A. Gondal, Appl. Catal. A **470**, 327 (2014)
14. X. Yu, V. De Waele, A. Löfberg, V. Ordomsky, A.Y. Khodakov, Nat. Commun. **10**, 700 (2019)
15. M.J. Boyd, A.A. Latimer, C.F. Dickens, A.C. Nielander, C. Hahn, J.K. Nørskov, D.C. Higgins, T.F. Jaramillo, ACS Catal. **9**, 7578 (2019)
16. B. Lee, T. Hibino, J. Catal. **279**, 233 (2011)
17. M. Ma, B.J. Jin, P. Li, M.S. Jung, J.I. Kim, Y. Cho, S. Kim, J.H. Moon, J.H. Park, Adv. Sci. **4**, 1700379 (2017)
18. A. Serov, I.V. Zenyuk, C.G. Arges, M. Chatenet, J. Power Sources **375**, 149 (2018)
19. H. Meng, D. Zeng, F. Xie, Catalysts **5**, 1221 (2015)
20. Z. Liu, E. Huang, I. Orozco, W. Liao, R.M. Palomino, N. Rui, T. Duchoň, S. Nemšák, D.C. Grinter, M. Mahapatra, P. Liu, J.A. Rodriguez, S.D. Senanayake, Science **368**, 513 (2020)
21. C. Wang, Y. Cao, H. Wang, Chemosphere **230**, 278 (2019)
22. L. Qin, M. Guo, Y. Liu, Z. Cheng, J.A. Fan, L.-S. Fan, Appl. Catal. B **235**, 143 (2018)
23. M. Álvarez, P. Marín, S. Ordóñez, Mol. Catal. **487**, 110886 (2020)
24. S.R. Chowdhury, P. Mukherjee, S.K. Bhattachrya, Int. J. Hydrog. Energy **41**, 17072 (2016)
25. H. Xiao, W.A. Goddard, T. Cheng, Y. Liu, Proc. Natl. Acad. Sci. **114**, 6685 (2017)
26. G.M. Tomboc, S. Choi, T. Kwon, Y.J. Hwang, K. Lee, Adv. Mater. **32**, 1908398 (2020)
27. I.H. Boyaci, H.E. Genis, B. Guven, U. Tamer, N. Alper, J. Raman Spectrosc. **43**, 1171 (2012)
28. R.S. Hyam, J. Lee, E. Cho, J. Khim, H. Lee, J. Nanosci. Nanotechnol. **12**, 8396 (2012)
29. A. Serov, U. Martinez, A. Falase, P. Atanassov, Electrochem. Commun. **22**, 193 (2012)
30. L. Yang, D. Yan, C. Liu, H. Song, Y. Tang, S. Luo, M. Liu, J. Power Sources **278**, 725 (2015)
31. C. Ji, S.-N. Yin, S. Sun, S. Yang, Appl. Surf. Sci. **434**, 1224 (2018)
32. D. Duan, H. Liu, Q. Wang, Y. Wang, S. Liu, Electrochim. Acta **198**, 212 (2016)
33. Y.-H. Wang, J.-B. He, Electrochim. Acta **66**, 45 (2012)
34. S.T. Mayer, J. Electrochem. Soc. **139**, 426 (1992)
35. G. Nogami, Y. Nishiyama, H. Nakamura, J. Electrochem. Soc. **135**, 877 (1988)
36. L.M.S. Garcia, S. Rajak, K. Chair, C.M. Godoy, A.J. Silva, P.V.R. Gomes, E.A. Sanches, A.S. Ramos, R.F.B. De Souza, A. Duong, A.O. Neto, ACS Omega **5**, 16003 (2020)
37. R. Zhou, Y. Zheng, M. Jaroniec, S.-Z. Qiao, ACS Catal. **6**, 4720 (2016)
38. B. Lee, Y. Sakamoto, D. Hirabayashi, K. Suzuki, T. Hibino, J. Catal. **271**, 195 (2010)
39. J. Nandenha, I. Nagahama, J. Yamashita, E. Fontes, J. Ayoub, R. de Souza, F. Fonseca, A. Neto, Int. J. Electrochem. Sci **14**, 10819 (2019)
40. J. Nandenha, E.H. Fontes, R.M. Piasentin, F.C. Fonseca, A.O. Neto, J. Fuel Chem. Technol. **46**, 1137 (2018)
41. Y. Kanazawa, K. Nukada, Bull. Chem. Soc. Jpn. **35**, 612 (1962)
42. P.A. Christensen, D. Linares-Moya, J. Phys. Chem. C **114**, 1094 (2010)
43. V.F. de Carmargo, E.H. Fontes, J. Nandenha, R.F.B. de Souza, A.O. Neto, Res. Chem. Intermed. **46**, 1555 (2020)
44. F. de MouraSouza, R.F.B. de Souza, B.L. Batista, M.C. dos Santos, F.C. Fonseca, A.O. Neto, J. Nandenha, Res. Chem. Intermed. **46**, 2481 (2020)